Coprecipitation of Fe/Cr Hydroxides at Organic-Water Interfaces: Functional Group Richness and (De)protonation Control Amounts and Compositions of Coprecipitates

Yandi Hu*[,†,&], Xulin Jiang[†], Suona Zhang[†], Dawei Cai[†], Zehao Zhou[†], Chuan Liu[†], Xiaobing Zuo[§], and Sang Soo Lee[‡]

[†]The Key Laboratory of Water and Sediment Sciences, Ministry of Education; State Environmental Protection Key Laboratory of All Material Fluxes in River Ecosystems; College of Environmental Sciences and Engineering, Peking University, Beijing 100871, P. R. China

[&]Southwest United Graduate School, Kunming 650092, China

[§]X-ray Science Division, Argonne National Laboratory, Lemont, IL 60439, United States

[‡]Chemical Sciences and Engineering Division, Argonne National Laboratory, Lemont, IL 60439, United States

*To Whom Correspondence Should Be Addressed

E-mail: huyandi@pku.edu.cn

Submitted to:

Environmental Science & Technology

Word count: Text (5274) + 1 Table (300) + 4 Figures (1200) = 6774 (limit of 7000)

TABLE OF CONTENTS FIGURE (Size: 3.33″ × 1.875″)

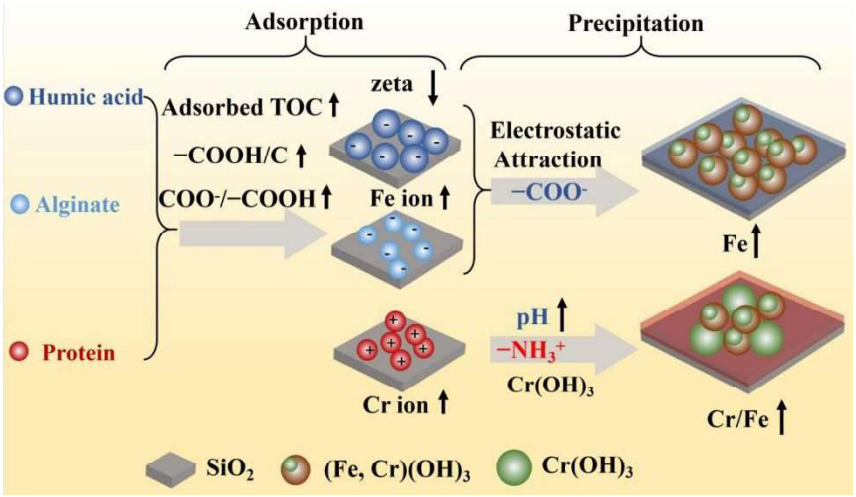

ABSTRACT

Iron/chromium hydroxide coprecipitation controls the fate and transport of toxic chromium (Cr) in many natural and engineered systems. Organic coatings on soil and engineered surfaces are ubiquitous; however, mechanistic controls of these organic coatings over Fe/Cr-hydroxide coprecipitation are poorly understood. Here, Fe/Cr-hydroxide coprecipitation was conducted on model organic coatings of humic acid (HA), sodium alginate (SA), and bovine serum albumin (BSA). The organics bonded with SiO_2 through ligand exchange with carboxyl (–COOH), and the adsorbed amounts and pK_a values of –COOH controlled surface charges of coatings. The adsorbed organic films also had different complexation capacities with Fe/Cr ions and Fe/Cr hydroxide particles, resulting in significant differences in both the amount (on HA>SA(–COOH)>>BSA(–NH_2)) and composition (Cr/Fe molar ratio: on BSA(–NH_2)>>HA>SA(–COOH)) of heterogeneous precipitates. Negatively charged –COOH attracted more Fe ions and oligomers of hydrolyzed Fe/Cr species and subsequently promoted heterogeneous precipitation of Fe/Cr hydroxide nanoparticles. Organic coatings containing –NH_2 were positively charged at acidic pH because of the high pK_a value of the functional group, limiting cation adsorption and formation of coprecipitates. Meanwhile the higher local pH near –NH_2 coatings promoted the formation of $Cr(OH)_3$. This study advances fundamental understanding of heterogeneous Fe/Cr hydroxide coprecipitation on organics, which is essential for successful Cr remediation and removal in both natural and engineered settings, as well as the synthesis of Cr-doped iron (oxy)hydroxides for material applications.

Synopsis: Functional groups of organics control amounts and compositions of Fe/Cr hydroxide coprecipitates by tuning local pH, ion complexation, and electrostatic interactions.

Keywords: Fe/Cr coprecipitation on organics, amine and carboxyl (de)protonation, local pH, ion complexation, electrostatic interactions

INTRODUCTION

Formation of Fe/Cr hydroxide co-precipitates (as (Fe, Cr)$(OH)_3$) play an important role in many natural environments and engineered systems. The Cr released into the environment through both natural and anthropogenic activities poses great health risks to plants, animals and humans.[1, 2] Compared with Cr(III), Cr(VI) is appreciably more toxic and mobile.[3] For the development of an efficient Cr detoxication strategy, iron(0/II)-based materials have been used for Cr(VI) reduction and concurrent Fe(III)/Cr(III) co-precipitation in both Cr contaminated soils and industrial Cr(VI) wastewater treatment.[4, 5] During metal/Fe hydroxide coprecipitation, metals (e.g., Cr, Al, etc.) can be sequestered in Fe hydroxides through structural incorporation, surface adsorption and surface precipitation.[6] These coprecipitates can occur in various sizes, compositions, and structures depending on the formation mechanisms and pathways.[7-10] At contaminated sites, (Fe, Cr)$(OH)_3$ coprecipitates could form either in solution as colloids (homogeneous nucleation) or on solid surfaces (heterogeneous nucleation).[11, 12] Homogeneously nucleated particles can move freely with flow resulting in colloidal transport of Cr; also, they can deposit onto solid surfaces. The deposits together with heterogeneously nucleated particles are heterogeneous coprecipitates, which can cause Cr immobilization in various environments (e.g., soils or groundwater). Thus, for better Cr sequestration, it is important to understand the mechanisms controlling heterogeneous coprecipitation of (Fe, Cr)$(OH)_3$.

In both natural and engineered settings, organic matter (OM) is ubiquitous either as dissolved colloidal phases or as coatings on solids.[13-15] Most previous studies of (Fe, Cr)$(OH)_3$ coprecipitation with organics are focused on homogeneous Fe/Cr-OM coprecipitation, usually performed with batch reactor experiments by monitoring changes in aqueous dissolved Fe/Cr ion concentrations.[16-18] Ning et al. investigated homogeneous (Fe, Cr)$(OH)_3$ coprecipitation with

varied carboxyl (–COOH)-containing model organics, and found that the complexation capability of organics with Fe/Cr ions controlled the amount and composition (i.e., Cr/Fe ratio) of the coprecipitates.[16] Yang et al. investigated homogeneous Fe/Cr coprecipitation in the presence of dissolved natural organic matter (NOM) with different origins, and revealed the significant role of –COOH in Cr complexation and incorporation into organo-ferrihydrite coprecipitates with molecular-level structural analysis.[17, 18] Few studies have looked into the heterogeneous precipitation (nucleation and deposition) of $Fe(OH)_3$ at organic-water interfaces.[19, 20] Ray et al. investigated pure $Fe(OH)_3$ nanoparticle precipitation on model organic-coated substrates and revealed a significant role of organic coatings' hydrophilicity and surface charge in altering the size/amount of heterogeneous precipitates.[19] Zhang et al. investigated (Fe, Cr)$(OH)_3$ coprecipitation onto bare and NOM-coated SiO_2/Al_2O_3, and preferential NOM adsorption onto Al_2O_3 over SiO_2 was found to greatly alter the amount/size/composition of the coprecipitates on Al_2O_3.[20] These previous studies shed light on the important role of organics in controlling (Fe, Cr)$(OH)_3$ coprecipitation through preferential adsorption in soil as coatings and complexation/electrostatic interactions with Fe/Cr ions, Fe/Cr hydroxide polymers and particles. NOM is a complex mixture of different components including humic substances, polysaccharides and proteins. Different adsorption behaviors of model organics onto varied soil surfaces (e.g., SiO_2 and Al_2O_3 representing Si-O and Al-O minerals of soils) have been reported.[21-23] Humic acid (HA) and sodium alginate (SA), representing humic substances and polysaccharides in NOM, were reported to have less adsorption onto SiO_2 than onto Al_2O_3.[21, 23] Bovine serum albumin (BSA), representing proteins in NOM, was found to adsorb more onto SiO_2 than HA.[24] However, the underlying mechanism controlling the adsorption capacities of varied OM compositions onto soil surfaces was not well understood. After adsorption onto soils,

the varied organic coatings may affect heterogeneous Fe/Cr hydroxide coprecipitation on soils in many ways. For instance, it has been widely reported that carboxyl groups (–COOH) in OM have a large affinity to Fe^{3+}/Cr^{3+} ions, hydrolyzed Fe/Cr species and Fe/Cr hydroxide particles.[18, 25-27] In another work, amine ($–NH_2$) functionalized mesoporous silica surfaces was reported to enhance Cr adsorption as compared to bare-silica due to Cr–NH_2 coordination.[28] In addition, distinct pK_a values of carboxyl and amine functional groups were reported,[29] thus their varied surface protonation/deprotonation processes can alter the surface charge of coated minerals and modify the structure of the electrical double layer near the interface, thus may alter the hydrolysis of Fe or Cr ions to form $Fe(OH)_3$ monomers, the oligomerization to form dimer/polymers, and finally Fe/Cr hydroxide coprecipitation. These previous studies indicated that varied OM compositions in NOM as coatings on soils may control heterogeneous (Fe, Cr)$(OH)_3$ coprecipitation in different ways, and that varied functional groups (mainly carboxyl and amine) in OM may play great roles in controlling OM adsorption onto soils and OM complexation with Fe/Cr ions and Fe/Cr hydroxide polymers/particles. However, Fe/Cr hydroxide coprecipitation onto Oms with varied functional groups was not studied yet, and the controlling mechanisms were largely unknown.

This study aimed to fill the important knowledge gap. HA, SA, and BSA with representative functional groups (mainly carboxyl and amine) were selected as model organics to represent humic substances, polysaccharides, and proteins as major components of NOM.[24] To further look into the roles of functional groups, self-assembled films (SAFs) terminated with –COOH and $–NH_2$ were also used to coat SiO_2. Surface properties of coatings, such as charges, roughness, hydrophobicity, and functional group richness, were thoroughly characterized. The amount, composition and size of Fe/Cr hydroxide coprecipitates formed on varied coatings and

Fe/Cr ion adsorption were also quantified for understanding the mechanisms. The distinct properties of functional groups (e.g., carboxyl richness, pK_a values, hydrophobicity, etc.) were found to greatly alter properties of SiO_2 after OM adsorption, and thus controlling the amount and composition of the heterogeneous coprecipitates and Cr stability.

EXPERIMENTAL SECTION

Preparation of model organic stock solutions. Model organic (i.e., HA, SA and BSA) powders were purchased from Sigma Aldrich, and there could be many differences between NOM in natural soil environment and the model organics we used here. Model OM powders were added into ultrapure water, and the solutions were put on tube rotators overnight and were then filtered with 0.45 μm PES filters. The dissolved organic carbon concentrations in filtrates were measured with total organic carbon analyzer (TOC-L, SHIMADZU, Japan), and filtrates were stored in refrigerator and used as stock solutions. The C, H, N, S contents of model OMs were determined using an elemental analyzer (Leeman EA3000, America), and their O contents were calculated by mass difference[30].

Bare SiO_2 substrate preparation. Silica powders (both micro- and nano-sized SiO_2) and glass coupons, which were suitable for different characterizations, were used as SiO_2 substrates for organic coatings and the following Fe/Cr ion adsorption and heterogeneous (Fe, Cr)$(OH)_3$ coprecipitation experiments (details in Figure S1 of Supporting Information). Silica powders with the grain size of 85 μm (Aladdin Co., China) and 20-50 nm (Zhejiang Hongsheng Material Technology Co., China) were purchased, with their properties shown in Table S2 of Supporting Information. Glass coupons were prepared by cutting 1 mm thick glass slides (VWR) into 1.25 cm × 5 cm. Both types of substrates were cleaned by first soaking in 10% HNO_3 overnight for leaching Fe/Cr ions from substrate surfaces, and a following leaching in 2% HNO_3 overnight

showed negligible amounts of Fe/Cr ions leached from the pretreated substrates. Then, the substrates were burned in oven at 500 °C for 2 hours to remove water, residual HNO_3 and all organics.

Preparation and characterization of organic coatings on substrates. Model organic solutions with 10 mg C/L were prepared with their stock solutions. The pH of prepared model organic solutions was adjusted to 3.2 with HNO_3, the same pH as the precipitation experiments. Then cleaned SiO_2 powders or coupons were added to allow model organic (HA/SA/BSA) adsorption as coatings, by mixing SiO_2 (50 g/L for micro-sized, or 5 g/L for nano-sized powder, or one piece of 1.25 cm × 5 cm × 0.1 cm coupon) in 10 mg C/L model organic solutions on tube rotators for 24 h.

To separately examine the roles of –COOH and $–NH_2$ functional groups, (3-Triethoxysilyl) propyl succinic anhydride (TSA, Gelest Inc.) and (3-Aminopropyl) triethoxysilane (APTS, Sigma-Aldrich) were used as precursors for –COOH and $–NH_2$ functionalization. To prepare SAF coatings on SiO_2 terminated with carboxyl (–COOH) and amine ($–NH_2$) functional groups, cleaned SiO_2 1.25 cm × 5 cm coupons or powders (2 g for micro-sized, or 0.2 g for nano-sized) were immersed in 10 mL solutions with 20 wt% precursor (TSA and APTS for –COOH and $–NH_2$ coatings, respectively) and 80 wt% toluene for 24 h. Then, the coupons were thoroughly rinsed with acetone and dried with N_2 to remove the loosely attached molecules. The powders were cleaned by acetone followed by ultrapure water for 3 times to remove the loosely attached molecules, and finally were dried in oven at 50 ℃ overnight.

Physicochemical properties of bare- and organic coated-SiO_2 powders/coupons, which were suitable for different characterizations, were thoroughly characterized using various techniques. The amounts of model organics (HA/SA/BSA) adsorbed onto 85 μm SiO_2 powders were

measured using a TOC analyzer. Micro-sized powders were used here for easier separation from solution than nano-sized powders, and for more organic adsorption than glass coupons. Also, the adsorbed HA/SA/BSA amounts on glass coupons as coatings were too little to cause measurable changes of TOC in solution before and after adsorption and were thus quantified using X-ray reflectivity (XR) measurements at beamline 33-BM-C at Advanced Photon Source (APS), Argonne National Laboratory (ANL), USA. Details of XR data analysis is available in our previous publication[31]. The surface charges of nano-sized powders with both model organic coatings and SAF (–COOH and $–NH_2$) coatings were measured using dynamic light scattering (DLS, Zetasizer, Nano ZS90, Malvern, UK) with a folded capillary cell (DTS1070, Malvern, UK). Fourier transform infrared spectra (FTIR) of model OM solutions (HA/SA/BSA) at varied pH conditions, as well as HA/SA/BSA coatings on nano-sized powders (with control sample of bare SiO_2 powder), were collected with IRTracer-100 (SHIMADZU, Japan) to characterize functional group (de)protonation of organics in solution and on substrates. Nano-sized powders were used here to maximize organic adsorption and strengthen DLS/FTIR signals. With flat glass coupons, the changes in hydrophobicity and surface roughness (Ra, nm) with varied organic coatings were measured using contact angle instrument (Biolin THETA, Sweden) and atomic force microscopy (AFM, Bruker Icon, USA), respectively.

Fe/Cr-hydroxide coprecipitation and Fe/Cr ion adsorption. Fe/Cr hydroxide coprecipitation experiments were conducted on tube rotators with freshly mixed solution containing 0.5 mM $Fe(NO_3)_3$ and $Cr(NO_3)_3$ in the presence of organic-coated SiO_2 coupons or powders. At the end of the 24 h reaction, heterogeneous coprecipitates on glass coupons were taken out from solution and the precipitates on organic-coated micro-sized SiO_2 were collected by centrifugation. Then, the coupons or powders were soaked in 2% HNO_3 on tube rotators for 24 h, and the dissolved Fe

or Cr ions were measured using inductively coupled plasma-mass spectrometry and inductively coupled plasma-optical emission spectrometer (ICP-MS/OES, Thermo Fisher, USA). During Fe/Cr hydrolysis and coprecipitation reactions which produced protons, the pH of the solution quickly decreased. The initial pH of the solution was calculated to be 3.2 by the Geochemist's Workbench (GWB, student version). To investigate the effects of functional groups' (de)protonation of OM coatings, solution pH changes during the first 1 h coprecipitation reactions were monitored with –COOH and $–NH_2$ coated nano-sized SiO_2 to maximize the coating effects.

To investigate the mechanisms of Cr sequestration (i.e., surface adsorption, surface precipitation, and structural incorporation) in Fe/Cr hydroxide coprecipitates, a layer-by-layer leaching experiment was also conducted with the heterogeneous coprecipitates. It was reported that surface enriched Cr (i.e., adsorbed Cr ions and surface $Cr(OH)_3$ precipitates) could be released with dilute HNO_3 (pH = 3) while Cr incorporated into the lattice structure of $(Fe, Cr)(OH)_3$ coprecipitates could not.[32] Here the heterogeneous Fe/Cr hydroxide coprecipitates on organic-coated SiO_2 were immersed in 4 mL dilute HNO_3 solution at pH = 3 and shaken for 1 hour at room temperature, followed by centrifugation for the collection of filtrates. Such 1 h leaching was repeated for 5 cycles followed by a 24 h leaching at pH 3, to collect the surface adsorbed Cr ions and surface $Cr(OH)_3$ precipitates. Finally, the remaining heterogeneous coprecipitates were immersed in 4 mL 2% HNO_3 solution at room temperature and shaken for 24 hours for complete dissolution. The Fe/Cr amounts in all collected filtrates after leaching and in the final dissolution solution were measured with ICP-MS/OES.

To further understand the coprecipitation mechanisms, two sets of Fe/Cr ion adsorption experiments onto varied organic coatings were also conducted. With HA/SA/BSA coated SiO_2

micro-sized powders, competitive Fe/Cr ion adsorption experiments were conducted following protocols similar to the coprecipitation experiments, except for a much lower initial concentration of 0.01 mM Fe and Cr to avoid Fe precipitation. With –COOH and $–NH_2$ coated SiO_2 coupons, Cr adsorption was performed with 0.5 mM Cr (the same Cr concentration as the coprecipitation experiments), with $NaNO_3$ and slight amount of HNO_3 added for adjusting ionic strength and solution pH to be the same as the coprecipitation experiments. As can be seen in Table S1 in Supporting Information, the complexation constants of organic matters (OMs) with divalent ions (Ca, Mg, Zn and Cu) are much smaller than the complexation constants of OMs with trivalent ions (Fe, Al and Cr); therefore, these common divalent cations may not affect greatly the complexation of Fe/Cr ions with OMs.

Size measurements of precipitates. The sizes of (Fe, Cr)$(OH)_3$ coprecipitates on organic-coated surfaces were characterized using grazing-incidence small-angle X-ray scattering (GISAXS) measurements at beamline 12 ID-B at APS in ANL. The original 2D GISAXS images were converted to 1D curves through linecuts using Matlab. Fitting of the 1D scattering curves was conducted using Irena SAS Igor macro.[33] More details regarding GISAXS data acquirement and analysis can be found in our previous work.[34-36] To understand the size difference of $Fe(OH)_3$ or $Cr(OH)_3$ precipitates, the z-average hydrodynamic diameters of pure $Fe(OH)_3$ or $Cr(OH)_3$ precipitates formed from 0.5 mM Fe or Cr nitrate solutions were measured by dynamic light scattering (DLS) in deionized (DI) water using a Malvern Zetasizer Nano ZS instrument (Malvern Instruments, Worcestershire, UK), with pH adjusted to be in the range of 3.2-7.0 with NaOH.

RESULTS AND DISCUSSION

Functional group richness and pK_a of adsorbed OMs controlled surface charge of OM-coated SiO_2. Amounts of model organics adsorbed onto SiO_2 varied, following the same order of HA > SA ≈ BSA based on both TOC and XR measurements for powder and coupon samples (Figure S2 and Table 1), indicating that size and shape of silica may not affect OM adsorption on them greatly. The amounts of –COOH and $–NH_2$ terminated SAF coatings onto SiO_2 could not be quantified due to its specific coating protocols described in the Experimental Section. Instead, changes in surface properties (e.g., surface zeta potential and contact angle, Table 1 and Figure S3 in Supporting Information) were monitored to confirm the formation of the model OM and SAF coatings at the interfaces.

FTIR spectra for both bare- and OM-coated SiO_2 were compared to reveal adsorption mechanisms (Figure 1). For bare-SiO_2, the peak around 1635 cm^{-1} cm (indicated by the grey bar in Figure 1) was assigned to free molecular H_2O by literatures.[37] After the adsorption of HA/SA as coatings, additional peaks (indicated by the red and orange bars in Figure 1) around 1540 and 1410 cm^{-1} appeared. According to literatures, these peaks represent asymmetric and symmetric vibrations of deprotonated carboxyl (COO^-), respectively.[38] The 1540 cm^{-1} peak (indicated by the red bar) was detected with HA/SA solutions at pH 7.0 but not at pH 3.2, indicating that the ratio of deprotonated to protonated carboxyl of HA/SA was low at pH 3.2. After HA/SA adsorption onto SiO_2 at pH 3.2, this deprotonated carboxyl (COO^-) peak at 1540 cm^{-1} appeared. Ligand exchange reaction of carboxyl in OMs with hydroxyl on the SiO_2 surface has been reported, which could result in carboxyl deprotonation.[24] Appearance of the deprotonated carboxyl peak after HA/SA adsorption indicated ligand exchange between carboxyl groups of HA/SA and SiO_2 substrates. The 1410 cm^{-1} peak (indicated by the orange bar) appeared for HA/SA solutions at

both pH conditions as well as after HA/SA adsorption onto SiO_2. Similar observations were consistent with previous study.[38]

For the FTIR spectra with BSA, the regions of 1600–1700 and 1500–1600 cm^{-1} represent amide I and II (indicated by the grey and red bars in Figure 1), respectively. The peaks at 1410 cm^{-1} (indicated by the orange bar in Figure 1) could be assigned to carboxyl, which were detected for BSA solution at both pH conditions as well as after BSA adsorption onto SiO_2. These observations were consistent with previous work investigating BSA adsorption onto SiO_2 with FTIR, where adsorption amounts varied over the pH range of 2-8 without significant peak position changes.[39] These findings indicated that FTIR technique could not be used for identifying the exact complexation sites (i.e., carboxyl or amine) for BSA adsorption onto SiO_2. Electrostatic forces could potentially favor the adsorption of the positively charged BSA on negatively charged SiO_2 than negatively charged HA at our acidic pH condition. However, Fukuzaki et al. investigated BSA adsorption onto Al_2O_3 and SiO_2 at pH 3 and find that, surprisingly, adsorption of positively charged BSA was favored on positively charged Al_2O_3 over negatively charged SiO_2.[22] They explained that this is because carboxyl instead of amine of BSA formed bonds with Al_2O_3/SiO_2 surfaces.[22] All these comparisons unequivocally indicate that adsorption of all model OMs (HA/SA/BSA) onto SiO_2 occur mainly through the covalent bond of –COOH with SiO_2 surfaces.

We also compared FTIR spectra over varied pH conditions to evaluate the relative acidities of HA and SA solutions. As shown in Figure 1, the characteristic peak for protonated carboxyl at ~1730 cm^{-1} (indicated by the blue bar) was observed at pH 3.2 for HA. In contrast, such a peak only showed up at a lower pH of 2.0 for SA, indicating that the SA used here is a stronger acid (with a lower pK_a value) than HA used here.

At the acidic pH = 3.2, the surface charge of SiO_2 changed from negative to positive with $–NH_2$ coatings, while the surface became more negative with –COOH coatings (Table 1), due to the protonation of $–NH_2$ to from $–NH_3^+$ and partial deprotonation of –COOH to form $–COO^-$. The BSA coated surfaces were positively charged. For BSA molecules containing equal amounts of amine and carboxyl functional groups, the isoelectric point has been reported to be pH = 5.[40] Thus at pH = 3.2 here, more $–NH_3^+$ than $–COO^-$ would form, resulting in the net positive surface charge. For both HA and SA containing –COOH functional groups, similar zeta potentials were measured. Surface charge for HA/SA could be controlled by the amount of deprotonated carboxyl (COO^-) in coatings, which could be controlled by adsorbed total organic carbon amount (TOC), ratio of carboxyl to total organic carbon (defined as carboxyl richness: -COOH/TOC, α_1 in eqn. (1), calculated based on O/C ratios (Table 1) measured by the elemental analyzer), and ratio of deprotonated carboxyl to total carboxyl (defined as carboxyl deprotonation fraction (α_2) in eqn. (2), indicated by pK_a values). For HA, with more adsorbed total organic carbon amount (TOC) than SA (Table 1), and lower α_1 and α_2, the surface deprotonated carboxyl could be similar in these two coatings, resulting in similar zeta potentials.

$$\alpha_1 = \frac{COOH_{tot}}{TOC} \quad (1)$$

$$\alpha_2 = \frac{COO^-}{COOH_{tot}} \quad (2)$$

Ion adsorption and zeta potential determined amount of (Fe, Cr)$(OH)_3$ coprecipitates on coatings. The amounts (as Fe) and compositions (as Cr/Fe ratio) of co-precipitates formed on HA/SA/BSA/SAF-coated SiO_2 surfaces varied greatly, as shown in Figure 2a. The amounts of (Fe, Cr)$(OH)_3$ coprecipitates harvested on HA- and SA-SiO_2 were larger than on BSA-SiO_2.

Compared with heterogeneous co-precipitates formed on SAF-coated surfaces, more (Fe, Cr)$(OH)_3$ coprecipitates were obtained on COOH-SiO_2, while less on NH_2-SiO_2. The difference in precipitate amount might not be affected by the roughness of the film surfaces, which was found similar (~1 nm) among the OM coatings based on AFM measurements (Table 1 and Figure S4 in Supporting Information). Also, the consistent trends, i.e., more coprecipitates on HA/SA/–COOH coatings than on BSA/–NH_2 coatings, indicated that functional groups played a key role in controlling the heterogeneous coprecipitation amounts. Heterogeneous coprecipitation, including heterogeneous nucleation and particle deposition from aqueous solution, could be affected by Fe/Cr ion adsorption affecting local supersaturation, surface interfacial energy for nucleation, and electrostatic forces controlling deposition. To understand the controlling factors in enhanced coprecipitation with HA/SA and COOH coatings, we compared these three surface processes.

First, Fe ion adsorption onto HA/SA/BSA coatings was quantified at pH = 3.2, identical with the coprecipitation pH conditions, but with a much lower initial Fe concentration to avoid precipitation. The amounts of Fe ions adsorbed on the organic coatings followed a trend as HA> SA>>BSA (Figure 2b), which was consistent with that of heterogeneous precipitation amounts on these coatings (Figure 2a). This similarity indicated that preferential Fe ion adsorption on HA/SA to BSA played an important role in controlling the amount of heterogeneous (Fe, Cr)$(OH)_3$ coprecipitates. Interestingly, the trend of Fe ion adsorption was also consistent with that of adsorbed carboxyl on these coatings, instead of the total adsorbed carbon. For example, the adsorbed Fe ions and carboxyl groups on BSA coating were both lower than on SA although BSA had a higher adsorbed carbon (TOC, Table 1), due to the much lower carboxyl richness (O/C, Table 1) of BSA. This correlation between carboxyl density and Fe ion adsorption could

be due to carboxyl complexation with Fe ions and electrostatic attraction between the negatively charged carboxyl and Fe ions/polymers.

Second, after Fe ion adsorption onto organics, the polymerization of $Fe(OH)_3$ monomers could result in the formation of Fe hydroxide particles on the surfaces. These heterogeneous nucleation processes can be controlled by interfacial energy. According to the classic nucleation theory[41], hydrophobic coatings with higher organic-solution interfacial energy generally lower the energy barrier for heterogeneous nucleation. As shown in Figure S3 and Table 1, the contact angles of the coated substrates are higher than bare SiO_2, indicating that the coatings increased the hydrophobicity of the surfaces, which could lower the energy barrier and promote heterogeneous nucleation. For HA/SA coatings, the contact angles were 7.1° and 7.0°, similar to that of –COOH SAF coatings (8.5°). For BSA and $–NH_2$ coatings, the contact angles were much higher than those of HA/SA/–COOH coatings (Table 1), indicating much lower energy for heterogeneous nucleation on BSA/$–NH_2$ coatings. However, limited coprecipitates occurred on BSA/$–NH_2$ coatings, indicating that heterogeneous nucleation might not be the dominant mechanism in controlling total coprecipitation amount.

Attraction of Fe hydroxide polymers/particles from solution onto surfaces could also contribute to heterogeneous coprecipitates, and such attraction could be controlled by surface charges of the coatings. As the Fe hydroxide particles are positively charged at the acidic pH condition, a negative surface charge of the coatings could promote the attraction of Fe hydroxide polymers/particles onto surfaces through electrostatic attraction. Thus, compared with positively charged BSA/NH_2 coatings (Table 1), precipitation was promoted on negatively charged HA/SA/COOH coatings.

In summary, Fe uptake to the organic coatings is determined by the coverages of the carboxyl groups in the organic films, which in turn controls the local supersaturation and subsequently the amounts of heterogeneous precipitates at the interfaces. Surface charges of the organic coatings, determined by functional groups' pK_a values, also play an essential role in controlling the amounts of heterogeneous precipitates on coatings by altering electrostatic forces between coatings and the Fe hydroxide polymers/particles in solution.

NH_2 coating promoted $Cr(OH)_3$ formation and affected Cr mobilization. For heterogeneous co-precipitates at varied surfaces (Figure 2), the Cr/Fe ratio with NH_2-terminated SAF coating was much higher than COOH-SiO_2. Consistently, the Cr/Fe ratio of (Fe, Cr)$(OH)_3$ coprecipitates obtained on BSA-coated surfaces was also higher than that of HA- and SA-coated surfaces (Figure 2a), indicating the important roles of surface functional groups. Several processes could affect the Cr/Fe ratio during heterogeneous (Fe, Cr)$(OH)_3$ formation: Fe/Cr ions could be attracted towards the surface through preferential ion adsorption with certain functional groups, and Cr can be sequestered in (Fe, Cr)$(OH)_3$ coprecipitates through structural incorporation, surface adsorption and surface precipitation.[6] To understand the higher Cr/Fe ratio of the heterogeneous coprecipitates on BSA/–NH_2 coatings, roles of functional groups on these processes were compared in the following paragraphs.

First, the amounts of Cr ions adsorbed onto the –NH_2 terminated SAF coatings were higher than onto the –COOH coatings under the same pH of 3.2 at Cr concentration of 0.5 mM (Figure 2). Analogously, competitive Fe and Cr ion adsorption onto HA/SA/BSA coatings was quantified under the same pH of 3.2 and Fe/Cr ratio of 1 as the coprecipitation experimental conditions, but with a much lower initial Fe/Cr concentration to avoid precipitation. Significantly lower Cr adsorption over Fe was observed onto all OM coatings (Figure 2b), which could also cause the

much higher amounts of Fe(III) than Cr(III) in the coprecipitates (Figure 2a); besides, the much higher solubility of $Cr(OH)_3$ over $Fe(OH)_3$ could also cause the lower amounts of Cr in the coprecipitates over Fe. Consistent with the SAF coated surfaces, the ratios of adsorbed Cr/Fe ions onto BSA-coated surfaces were higher than those with HA- or SA- coatings. Promoted adsorption of positively charged Cr ions on positively charged BSA/–NH_2 surfaces indicated the insignificant role of electrostatic interaction. Previous study reported the promoted adsorption of Cr on –NH_2 functionalized surfaces compared with that on bare SiO_2,[28] where the direct coordination between –NH_2 and hydrolyzed Cr ions was found to account for the promotion through dynamic characterization of amine-Cr complexes.[28] The adsorption of hydrolyzed Cr species can be more favorable due to easier dissociation of water molecules from the species, reported as rate-limiting step for the complexation reaction.[42] In our recent study, Cr ion hydrolysis was found to be greatly affected by solution pH at acidic pH, e.g., the hydrolyzed Cr species including $Cr(OH)_2^+$ and $Cr(OH)_2^+$ was found to increase substantially with increasing local solution pH near Al_2O_3 surfaces.[20] Here, distinction in pK_a value between –COOH (1-3[29]) and –NH_2 (9-10[29]) may alter local solution pH through surface protonation or deprotonation. During the coprecipitation experiments, the solution pH was measured to decrease only slightly from 3.25 to 3.19 after 1 h reaction with –NH_2 coatings, while the solution pH quickly dropped to 2.80 with –COOH coatings (Figure S5). The smaller pH decrease with –NH_2 could be attributed to the protonation of –NH_2 under the current experimental conditions. In this perspective, local solution pH near –NH_2 coatings could be much higher than the pH of bulk solution, resulting in greatly promoted Cr hydrolysis and thus its adsorption on –NH_2/BSA coatings. For instance, our previous work showed that the hydrolyzed Cr species could increase from 16% to 42% with pH increase from 3.2 to 3.8. [20]

To identify the major mechanism of Cr sequestration (i.e., surface enrichment vs. structural incorporation), a layer-by-layer dissolution was conducted with the heterogeneous coprecipitates (Figure 3). In the first few cycles of the pH = 3.0 acid leaching for coprecipitates on $–NH_2$ and –COOH surfaces, much higher amount of Cr over Fe was released from the coprecipitates on $–NH_2$. The higher Cr/Fe ratio measured with the first few cycles of the acid washing indicated the greater surface enrichment of Cr in the coprecipitates on $–NH_2$ surfaces than those on the –COOH surfaces. In the following washing cycles and overnight dissolution, the ratios of released Cr/Fe ions from the coprecipitates on coatings remained constant and were similar between the $–NH_2$ and –COOH surfaces. This observation implied a similar extent of Cr incorporation into structure of (Fe, Cr)$(OH)_3$ coprecipitates. The Cr surface enrichment of the Fe/Cr hydroxide coprecipitates on $–NH_2$ surfaces could be due to Cr ion adsorption and/or $Cr(OH)_3$ particle formation. The ratio of adsorbed Cr/Fe ions on BSA was found to be 0.20 (Figure 2), which was only slightly higher than those on HA/SA (0.12 and 0.17). Such small differences could not explain the much larger differences in ratio (1.62 for –COOH, 6.23 for $–NH_2$, Figure 3) of Cr/Fe ions released from the coprecipitates on coatings during the initial leaching at pH = 3.0, indicating the formation of $Cr(OH)_3$ particles on $–NH_2$ coating. Although the bulk solution was undersaturated with respect to $Cr(OH)_3$, this solid phase might form near $–NH_2$ coated surfaces because of locally increased Cr ion concentration and higher pH. To test this hypothesis, heterogeneous coprecipitates on bare and organic-coated surfaces were measured using GISAXS. Specifically, a peak assigned to nanoparticles of ~4 nm were found at all surfaces, which could be the signal from (Fe, Cr)$(OH)_3$ nanoparticles. Remarkably, nanoparticles with larger sizes at ~9 nm were also found at $–NH_2$ and BSA surfaces (Figure 4). Nanoparticles with such larger sizes detected on $–NH_2$ surface could be $Cr(OH)_3$, as the

hydrodynamic sizes of $Cr(OH)_3$ particles were measured to be larger than those of $Fe(OH)_3$ formed in solutions under varied pH conditions (Figure S6).

In summary, the higher Cr/Fe ratio of the coprecipitates formed on BSA/NH_2-substrates should be ascribed to the higher pK_a value of the organic functional groups, leading to local solution pH increases through protonation, which could promote Cr hydrolysis, Cr ion adsorption, and $Cr(OH)_3$ formation. However, the adsorbed Cr ions (and $Cr(OH)_3$ surface precipitates) could be easily desorbed (and dissolved) at pH = 3.0. Therefore, although more Cr could be immobilized on –NH_2 coatings, such immobilization might be ineffective with decreasing solution pH. Zhu et al. investigated homogeneous Fe/Cr hydroxide coprecipitation with varied aqueous Cr/Fe ratios (1.5:1, 1:1, 1:4 and 1:9) in the presence of natural organic matter, and found that Cr/Fe ratio had slight effects on the sizes of Fe(III)-Cr(III) hydroxide coprecipitates and carbon removal, meanwhile it greatly affected Cr removal. Meanwhile, it greatly affected Cr removal, with lower efficiency for Cr removal from solutions with higher aqueous Cr/Fe ratios.[45] Effects of the Cr/Fe ratio on heterogeneous Fe(III)-Cr(III) coprecipitation on organic coatings can be an interesting future research.

ENVIRONMENTAL IMPLICATIONS

The formation of impurity-bearing Fe (oxy)hydroxides (e.g., ferrihydrite) on organic substrates has profound implications in both natural and engineered systems. Incorporation of Cr in (Fe, Cr)$(OH)_3$ coprecipitates could enhance its immobilization in the environment. To understand the role of organic functional groups on (Fe, Cr)$(OH)_3$ coprecipitation in soil, this work systematically investigated the amount as well as the composition of (Fe, Cr)$(OH)_3$ coprecipitates formed on substrates coated with varied organics, relevant to natural organic

matter and the engineered organic films. The amount of Fe in coprecipitates was positively correlated to the amount of Fe ion adsorption and the negative charge of the substrates, which are controlled by the richness and pK_a of surface carboxyls (–COOH). The surfaces modified with –NH_2 exhibited limited formation of (Fe, Cr)$(OH)_3$ due to the same positive charges between the surface and the particles. In contrast, the Cr/Fe ratio of the coprecipitates was higher, presumably because of the increased local pH due to the protonation of –NH_2 that promoted Cr adsorption and $Cr(OH)_3$ formation. The new knowledge revealed by this work is valuable for better understanding the sequestration and stability of Cr in the environment.

The heterogeneity of natural organic matters (NOM) made it hard to investigate their roles in many geochemical processes. The current work demonstrated that effects of varied organic coatings on the coprecipitation process were predominantly controlled by the different functional groups. Such findings of this study have broad implications for future studies of using model organic films with controlled functional groups to invest NOM coatings on soils.

In many engineered settings, metal-doping in nanomaterials is a widely adopted strategy to tune their properties as needed for various applications[43]. For example, Cr was doped in Fe oxides to improve their catalytic efficiency[44]. The information provided from our study might also help realize better design and application of impurity-doping ferrihydrite materials in different fields as adsorbents and catalysis.

ACKNOWLEDGMENTS

This work was supported by National Natural Science Foundation of China (Grant No.: 42177193), Science and Technology Project of Southwest United Graduate School of Yunnan (202302AP370002), and the U.S. Department of Energy (DOE), Office of Science, Office of Basic Energy Sciences, Geosciences program (S.S.L.) under Contract DE-AC02-06CH11357 to

UChicago Argonne, LLC as operator of Argonne National Laboratory (ANL) (for XR measurements, data analysis, and interpretation). GISAXS and XR measurements were performed at beamlines 12-ID-B and 33-BM-C, respectively, of the Advanced Photon Source, a U.S. DOE Office of Science User Facility operated for the DOE Office of Science by ANL under Contract No. DE-AC02-06CH11357.

ASSOCIATED CONTENT

Supporting Information

AFM, XR, and contact angle measurement data of bare and organic-coated substrates, DLS size measurements of pure $Fe(OH)_3$ and $Cr(OH)_3$ precipitates in solutions, and pH change during co-precipitation experiments are provided in SI. This information is available free of charge on the ACS Publications website.

AUTHOR INFORMATION

Corresponding Author

* e-mail: huyandi@pku.edu.cn.

Notes

The authors declare no competing financial interest.

Table 1. Surface properties of bare and organic coated SiO_2 measured at the same pH (i.e., 3.2, adjusted with HNO_3) as coprecipitation experiments.

Organic coatings	Zeta Potential (mV)	Contact Angle (°)	Roughness (AFM, nm)	Adsorbed C by TOC (μg C/g)	Adsorbed C by XR (μg C/cm^2)	O/C by elemental analyzer
SiO_2	-19.0 ± 0.8	1.9°	N/A	N/A	N/A	N/A
BSA	28.4 ± 0.9	72.5	1.1 ± 0.5	22 ± 5	0.17±0.04	0.469 ± 0.004
HA	-24.5 ± 0.3	7.1	0.7 ± 0.3	33 ± 5	0.27±0.08	1.217 ± 0.002
SA	-25.2 ± 0.6	7.0	0.8 ± 0.3	11 ± 6	0.11±0.05	1.967 ± 0.002
–COOH	-29.9 ± 0.6	8.5	1.4 ± 0.7	N/D	N/A	N/D
$–NH_2$	33.7 ± 0.7	29.0	0.2 ± 0.1	N/D	N/A	N/D

Figure 1. FTIR spectra of bare and organic-coated SiO_2. The spectra of model organics (HA, BSA, and SA) in different pH solutions were also collected for differentiating peak positions between protonated and deprotonated functional groups (–COOH and $–NH_2$).

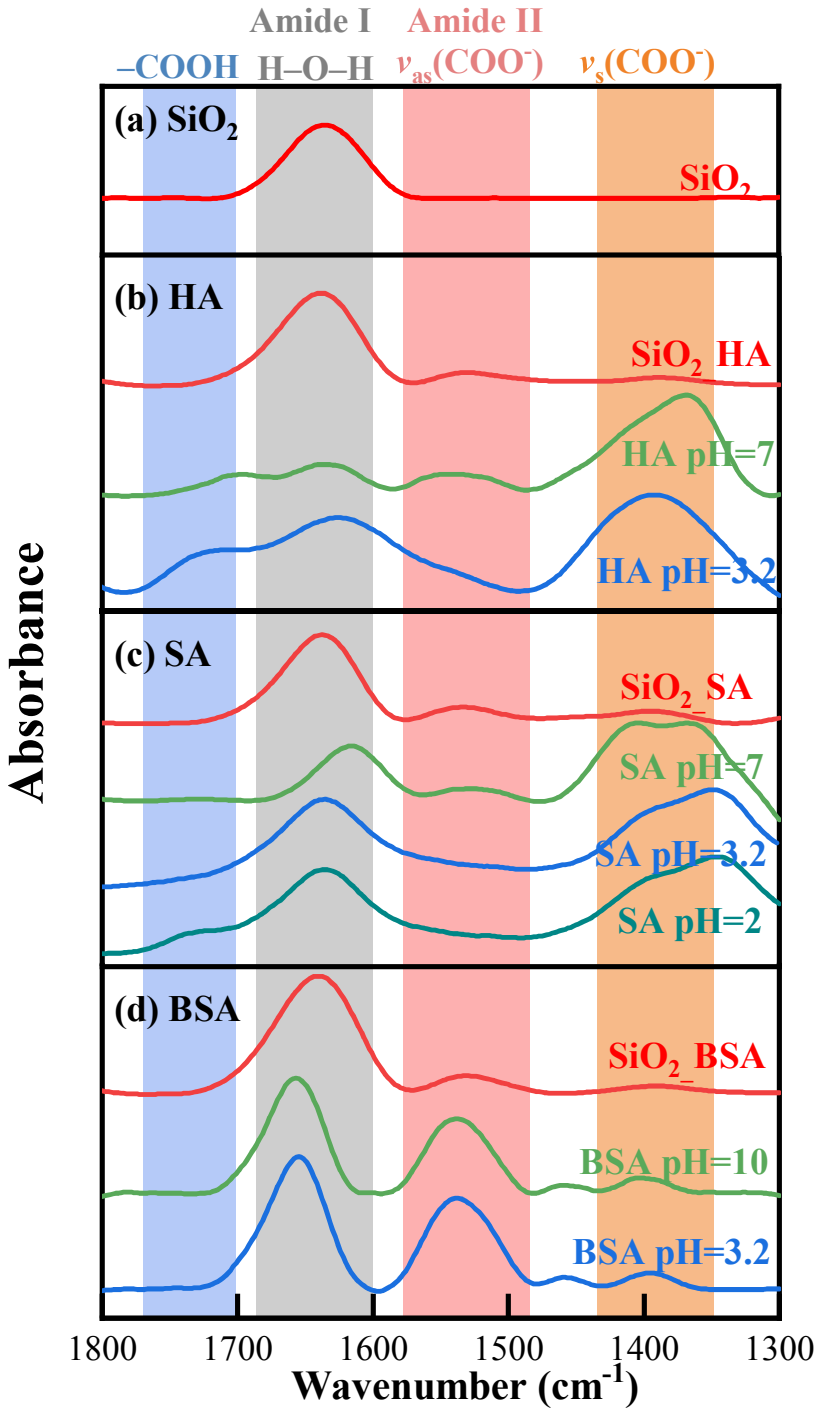

Figure 2. The amounts of Fe and Cr removed from initial solutions as heterogeneous (Fe, Cr)$(OH)_3$ precipitates or by adsorption on varied substrates and their molar ratios of Cr/Fe. a) Precipitation experimental conditions: initial $[Fe^{3+}]_0 = [Cr^{3+}]_0 = 0.5$ mM, pH ~3.2, 50 g/L HA, BSA or SA-coated SiO_2 powders, or 1.25 cm × 5 cm –COOH/–NH_2-coated SiO_2 coupons, reaction time = 24 h. b) Adsorption experimental conditions: initial $[Cr^{3+}]_0 = [Fe^{3+}]_0 = 0.01$ mM, pH ~3.2, 50 g/L HA, BSA or SA-coated SiO_2 powders, reaction time = 24 h. For experiments with 1.25 cm × 5 cm –COOH/–NH_2-coated SiO_2 coupons, only Cr adsorption with initial concentration of 0.5 mM was conducted, as 0.5 mM Fe(III) would precipitate.

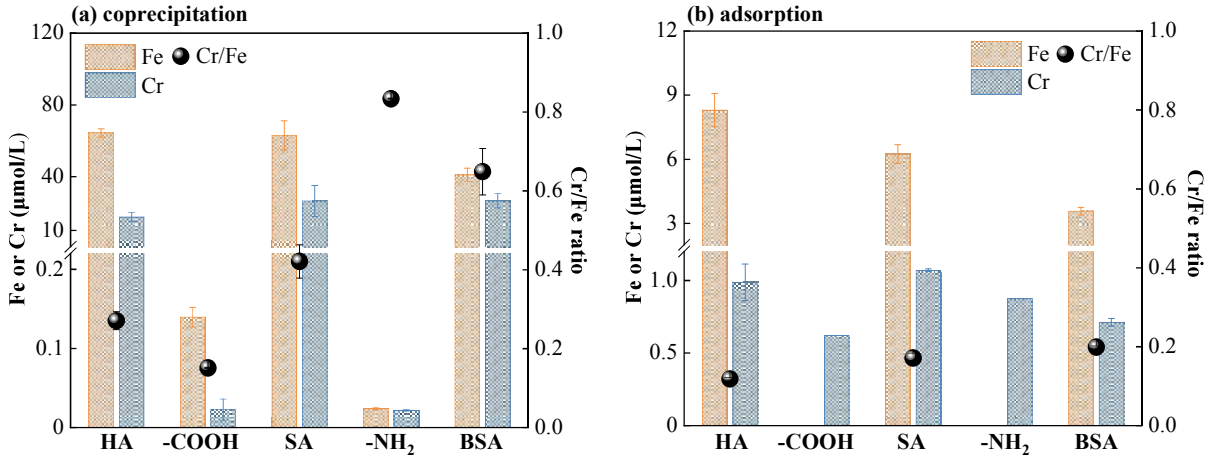

Figure 3. The concentrations of Fe and Cr and Cr/Fe ratio released during layer-by-layer washing cycles. The initial 6 cycles of acid washing were conducted with pH 3 HNO_3, and that of the last dissolution cycle was conducted with 2% HNO_3.

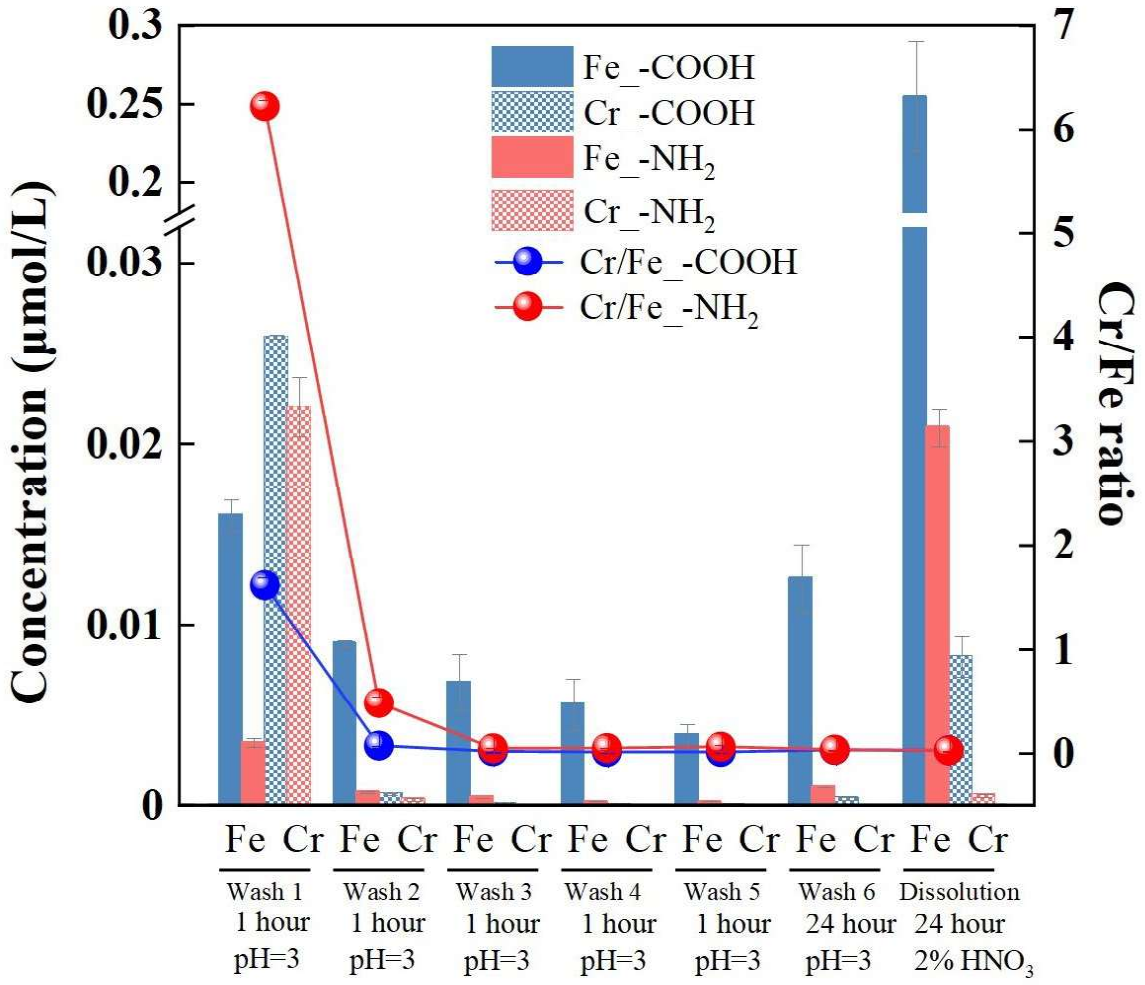

Figure 4. Scattering curves of *ex-situ* GISAXS measurements for (Fe, Cr)$(OH)_3$ nanoparticles formed on bare and organic-coated SiO_2. The colored open circles are the data and the solid or dashed lines are the best-fit curves using the spherical particle model and log-normal size distribution function. The average radii of the fitted nanoparticles are marked on the figures.

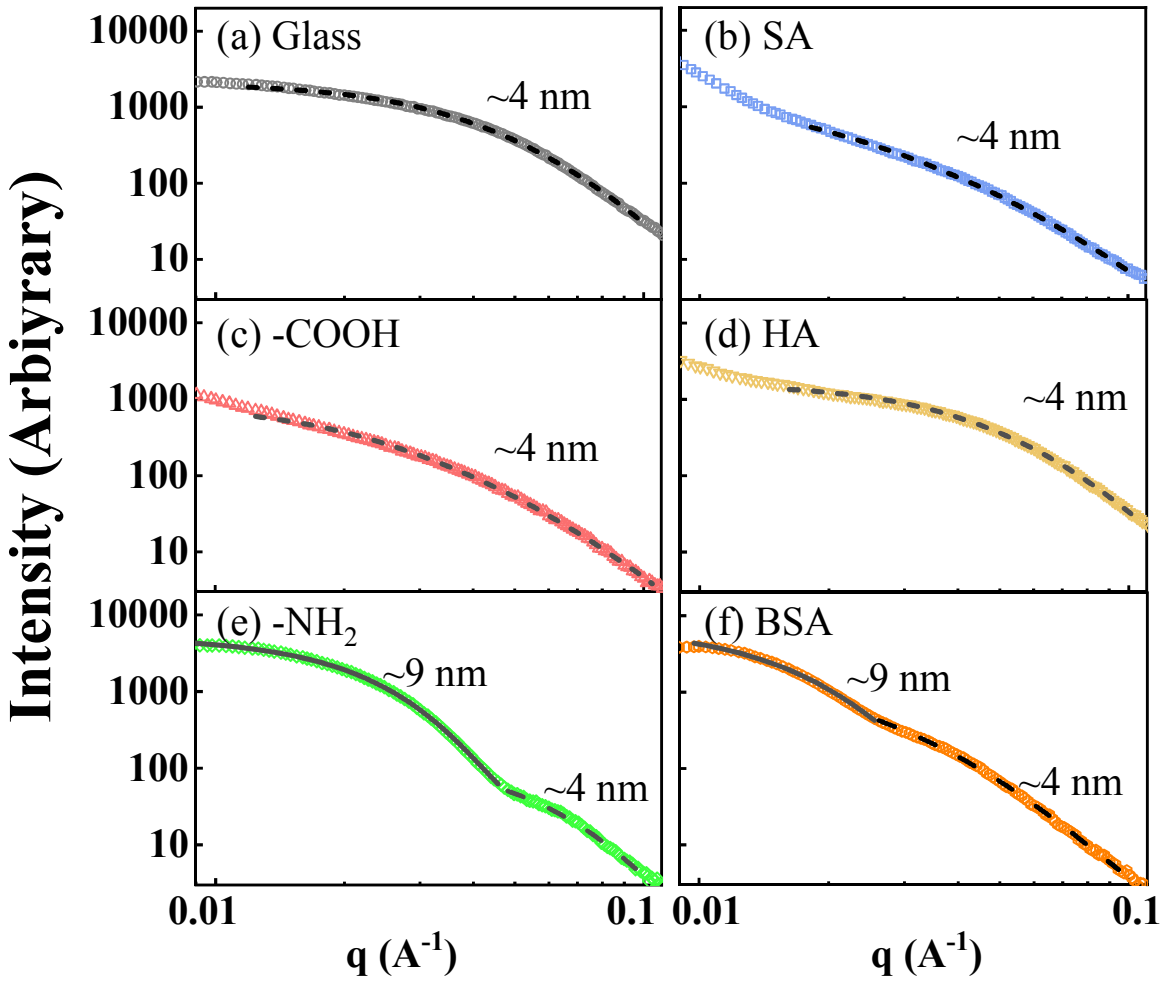

References:

1. Nriagu, J. O.; Pacyna, J. M., Quantitative assessment of worldwide contamination of air, water and soils by trace metals. *Nature* **1988,** *333*, (6169), 134-139.
2. Jobby, R.; Jha, P.; Yadav, A. K.; Desai, N., Biosorption and biotransformation of hexavalent chromium [Cr (VI)]: a comprehensive review. *Chemosphere* **2018,** *207*, 255-266.
3. Ao, M.; Chen, X.; Deng, T.; Sun, S.; Tang, Y.; Morel, J. L.; Qiu, R.; Wang, S., Chromium biogeochemical behaviour in soil-plant systems and remediation strategies: A critical review. *Journal of Hazardous Materials* **2021**, 127233.
4. Eary, L.; Rai, D., Chromate removal from aqueous wastes by reduction with ferrous ion. *Environmental Science & Technology* **1988,** *22*, (8), 972-977.
5. Gheju, M., Hexavalent chromium reduction with zero-valent iron (ZVI) in aquatic systems. *Water, Air, & Soil Pollution* **2011,** *222*, (1-4), 103-148.
6. Alvarez, M.; Rueda, H.; Sileo, E. E., Simultaneous incorporation of Mn and Al in the goethite structure. *Geochimica et Cosmochimica Acta* **2007,** *71*, 1009–1020.
7. Cismasu, A. C.; Michel, F. M.; Stebbins, J. F.; Levard, C.; Brown, G. E., Jr., Properties of impurity-bearing ferrihydrite I. effects of Al content and precipitation rate on the structure of 2-line ferrihydrite. *Geochimica Et Cosmochimica Acta* **2012,** *92*, 275-291.
8. Schulze, D. G., The influence of aluminum on iron-oxides. VIII. unit-cell dimensions of Al-substitted goethites and estimation of Al from them. *Clays and Clay Minerals* **1984,** *32*, (1), 36-44.
9. Bazilevskaya, E.; Archibald, D. D.; Martinez, C. E., Rate constants and mechanisms for the crystallization of Al nano-goethite under environmentally relevant conditions. *Geochimica et Cosmochimica Acta* **2012,** *88*, 167-182.
10. Cornell, R. M.; Schwertmann, U., The iron oxides: structure, properties, reactions, occurences and uses. Wiley-VCH: Darmstadt, 2003.
11. Dai, C.; Hu, Y., Fe(III) hydroxide nucleation and growth on quartz in the presence of Cu(II), Pb(II), and Cr(III): metal hydrolysis and adsorption. *Environmental Science & Technology* **2015,** *49*, 292−300.
12. Dai, C.; Zuo, X.; Cao, B.; Hu, Y., Homogeneous and heterogeneous precipitation of $(Fe_x, Cr_{1-x})(OH)_3$ nanoparticles: implications for aqueous Cr removal. *Environmental Science & Technology* **2016,** *50*, 1741-1749.
13. Aiken, G. R.; Hsu-Kim, H.; Ryan, J. N., Influence of dissolved organic matter on the environmental fate of metals, nanoparticles, and colloids. In American Chemical Society Publications: 2011.
14. Connell, D. W., *Basic concepts of environmental chemistry*. CRC Press LLC: 2005.
15. Nebbioso, A.; Piccolo, A., Molecular characterization of dissolved organic matter (DOM): a critical review. *Analytical and bioanalytical chemistry* **2013,** *405*, 109-124.
16. Deng, N.; Li, Z.; Zuo, X.; Chen, J.; Shakiba, S.; Louie, S. M.; Rixey, W. G.; Hu, Y., Coprecipitation of Fe/Cr Hydroxides with Organics: Roles of Organic Properties in Composition and Stability of the Coprecipitates. *Environmental Science & Technology* **2021,** *55*, (8), 4638-4647.
17. Xia, X.; Yang, J.; Yan, Y.; Wang, J.; Hu, Y.; Zeng, X., Molecular Sorption Mechanisms of Cr(III) to Organo-Ferrihydrite Coprecipitates Using Synchrotron-Based EXAFS and STXM Techniques. *Environmental Science & Technology* **2020,** *54*, (20), 12989-12997.

18. Yang, J.; Xia, X.; Liu, J.; Wang, J.; Hu, Y., Molecular Mechanisms of Chromium(III) Immobilization by Organo–Ferrihydrite Co-precipitates: The Significant Roles of Ferrihydrite and Carboxyl. *Environmental Science & Technology* **2020,** *54*, (8), 4820-4828.
19. Ray, J. R.; Lee, B.; Baltrusaitis, J.; Jun, Y.-S., Formation of Iron(III) (Hydr)oxides on Polyaspartate- and Alginate-Coated Substrates: Effects of Coating Hydrophilicity and Functional Group. *Environmental Science & Technology* **2012,** *46*, (24), 13167-13175.
20. Zhang, S.; Cheng, L.; Zuo, X.; Cai, D.; Tong, K.; Hu, Y.; Ni, J., (Fe, Cr)(OH)3 Coprecipitation in Solution and on Soil: Roles of Surface Functional Groups and Solution pH. *Environmental Science & Technology* **2023,** *57*, (19), 7516-7525.
21. Yang, K.; Lin, D.; Xing, B., Interactions of humic acid with nanosized inorganic oxides. *Langmuir* **2009,** *25*, (6), 3571-3576.
22. Fukuzaki, S.; Urano, H.; Nagata, K., Adsorption of bovine serum albumin onto metal oxide surfaces. *Journal of Fermentation and Bioengineering* **1996,** *81*, (2), 163-167.
23. Wang, Z.; Liu, D.-y.; Xiao, K.; Guan, J.; Xie, Y. F.; Wang, X.-m.; Waite, T. D., Role of adsorption in combined membrane fouling by biopolymers coexisting with inorganic particles. *Chemosphere* **2018,** *191*, 226-234.
24. Philippe, A.; Schaumann, G. E., Interactions of dissolved organic matter with natural and engineered inorganic colloids: a review. *Environmental science & technology* **2014,** *48*, (16), 8946-8962.
25. Eusterhues, K.; Rennert, T.; Knicker, H.; Kogel-Knabner, I.; Totsche, K. U.; Schwertmann, U., Fractionation of organic matter due to reaction with ferrihydrite: coprecipitation versus adsorption. *Environmental Science & Technology* **2011,** *45*, (2), 527-533.
26. Chen, C.; Dynes, J. J.; Wang, J.; Sparks, D. L., Properties of Fe-organic matter associations via coprecipitation versus adsorption. *Environmental Science & Technology* **2014,** *48*, (23), 13751-9.
27. Evanko, C. R.; Dzombak, D. A., Surface complexation modeling of organic acid sorption to goethite. *Journal of colloid and interface science* **1999,** *214*, (2), 189-206.
28. Egodawatte, S.; Datt, A.; Burns, E. A.; Larsen, S. C., Chemical insight into the adsorption of chromium (III) on iron oxide/mesoporous silica nanocomposites. *Langmuir* **2015,** *31*, (27), 7553-7562.
29. Pahari, S.; Sun, L.; Alexov, E., PKAD: a database of experimentally measured pK_a values of ionizable groups in proteins. *Database* **2019,** *2019*.
30. Yang, Y.; Shu, L.; Wang, X.; Xing, B.; Tao, S., Impact of de-ashing humic acid and humin on organic matter structural properties and sorption mechanisms of phenanthrene. *Environmental Science & Technology* **2011,** *45*, (9), 3996-4002.
31. Dai, C.; Stack, A. G.; Koishi, A.; Fernandez-Martinez, A.; Lee, S. S.; Hu, Y., Heterogeneous nucleation and growth of barium sulfate at organic–water interfaces: interplay between surface hydrophobicity and Ba2+ adsorption. *Langmuir* **2016,** *32*, (21), 5277-5284.
32. Edwards, M.; Benjamin, M. M., Regeneration and reuse of iron hydroxide adsorbents in treatment of metal-bearing wastes. *Water Pollution Control Federation* **1989**, 481-490.
33. Ilavsky, J.; Jemian, P. R., Irena: tool suite for modeling and analysis of small-angle scattering. *Journal of Applied Crystallography* **2009,** *42*, (2), 347-353.
34. Hu, Y.; Li, Q.; Lee, B.; Jun, Y. S., Aluminum affects heterogeneous Fe(III) (Hydr)oxide nucleation, growth, and ostwald ripening. *Environmental Science & Technology* **2014,** *48*, (1), 299-306.

35. Hu, Y.; Neil, C.; Lee, B.; Jun, Y.-S., Control of heterogeneous Fe (III)(hydr) oxide nucleation and growth by interfacial energies and local saturations. *Environmental Science & Technology* **2013,** *47*, (16), 9198-9206.
36. Hu, Y.; Lee, B.; Bell, C.; Jun, Y.-S., Environmentally abundant anions influence the nucleation, growth, ostwald ripening, and aggregation of hydrous Fe (III) oxides. *Langmuir* **2012,** *28*, (20), 7737-7746.
37. Hernández-Morales, V.; Nava, R.; Acosta-Silva, Y. J.; Macías-Sánchez, S. A.; Pérez-Bueno, J. J.; Pawelec, B., Adsorption of lead (II) on SBA-15 mesoporous molecular sieve functionalized with $-NH_2$ groups. *Microporous and Mesoporous Materials* **2012,** *160*, 133-142.
38. Cuba-Chiem, L. T.; Huynh, L.; Ralston, J.; Beattie, D. A., In situ particle film ATR FTIR spectroscopy of carboxymethyl cellulose adsorption on talc: binding mechanism, pH effects, and adsorption kinetics. *Langmuir* **2008,** *24*, (15), 8036-44.
39. Givens, B. E.; Diklich, N. D.; Fiegel, J.; Grassian, V. H., Adsorption of bovine serum albumin on silicon dioxide nanoparticles: Impact of pH on nanoparticle–protein interactions. *Biointerphases* **2017,** *12*, (2).
40. Rezwan, K.; Meier, L. P.; Rezwan, M.; Vörös, J.; Textor, M.; Gauckler, L. J., Bovine serum albumin adsorption onto colloidal Al_2O_3 particles: a new model based on zeta potential and UV− Vis measurements. *Langmuir* **2004,** *20*, (23), 10055-10061.
41. Lasaga, A. C., *Kinetic theory in the earth sciences*. Princeton university press: 1998.
42. Hamm, R. E.; Johnson, R. L.; Perkins, R. H.; Davis, R. E., Complex ions of chromium. VIII. Mechanism of reaction of organic acid anions with chromium (III) 1, 2. *Journal of the american chemical society* **1958,** *80*, (17), 4469-4471.
43. Wiesner, M.; Bottero, J.-Y., *Environmental nanotechnology*. McGraw-Hill Professional Publishing New York: 2007.
44. Keturakis, C. J.; Zhu, M.; Gibson, E. K.; Daturi, M.; Tao, F.; Frenkel, A. I.; Wachs, I. E., Dynamics of CrO_3–Fe_2O_3 catalysts during the high-temperature water-gas shift reaction: molecular structures and reactivity. *ACS Catalysis* **2016,** *6*, (7), 4786-4798.
45. Zhu, S.; Luo, W.; Mo, Y.; Ding, K.; Zhang, M.; Jin, C.; Wang, S.; Chao, Y.; Tang, Y.-T.; Qiu, R., New insights into the role of natural organic matter in Fe–Cr coprecipitation: importance of molecular selectivity. *Environmental Science & Technology* **2023,** *57*, (37), 13991-14001.